

Analyzing the Flow Field in the Oil Chamber of a Hydrostatic Guide Rail Used for Ultra-Precision Machining: Numerical Simulation and Performance Optimization

Youxin Li*

Department of Mechanical and Electrical Engineering, QingHai Higher Vocational & Technical Institute, Haidong, 810799, China

*Corresponding Author: Youxin Li. Email: xinwhut@163.com

Received: 14 December 2019; Accepted: 24 August 2020

Abstract: In order to explore the impact of different structural design parameters and environmental factors on the performance of the hydrostatic guide rail, the flow field inside its oil chamber is simulated, which provides direction and guidance for the design and optimization of the guide rail system. Based on the theory of fluid lubrication and the Reynolds equation, numerical simulations are performed through a mathematical model. The results suggest that the bearing capacity of the oil film increases with the oil supply pressure. The film thickness and the film stiffness share a positive correlation. Different oil film thickness and different input pressure parameters can have a significant impact on bearing capacity and oil film stiffness. The correlations identified in the present analysis can be used as a basis to optimize the guide rail design.

Keywords: Guide rail oil chamber; simulation; hydrostatic pressure; guide rail performance

1 Introduction

In recent years, with the rapid development of modern industry and high-tech technology, ultra-precision machining technology has become an essential direction of the equipment manufacturing industry [1]. The ultra-precision machining technology and micro nanomachine tools are researched and developed in combination with the significant developing needs of the manufacturing industry at this stage, aiming to achieve industrialization by developing critical components and equipment prototype with independent intellectual property rights [2]. The Micro-nano machine tool is the general term of machine tools for micro-nano-ultra precision machining, which represents the highest level of industrial technology in a nation. It is an essential cornerstone of the high-end manufacturing industry, determines the core competitiveness of a nation's overall manufacturing industry, and directly affects the national economy and people's livelihood [3].

The performance of the micro-nano-ultra precision machine tool mainly depends on the performance of its key components. As a crucial component of the machine tool system, the guide rails can directly affect the position and motion accuracy of the moving components of the machine tool [4]. The hydrostatic guide rail is common in micro-nano-ultra precision machine tools due to its advantages of high rigidity, high precision,



This work is licensed under a Creative Commons Attribution 4.0 International License, which permits unrestricted use, distribution, and reproduction in any medium, provided the original work is properly cited.

low wear, and long service life. The design of hydrostatic guide rail shall meet the requirements of high speed, high efficiency, and high precision. On the one hand, the guide rail must have enough static stiffness and excellent dynamic characteristics [5]; on the other hand, the oil film between guide rails shall have excellent oil film rigidity and bearing capacity [6]. Research on hydrostatic guide rail technology starts later in China, but it develops rapidly. Notably, of late years, with the joint efforts of universities, research institutes, and factories, the hydrostatic guide rail technology has made significant progress, and its application scope has been rapidly expanded to the manufacturing industry, civil and military equipment [7]. Hydrostatic guide rail technology has the advantages of excellent earthquake resistance, fast linear running speed, and significant stiffness, which can solve the creeping problem caused by the heavyweight of the transmission component in heavy machine tools. In China, hydrostatic guide rail has been applied in various numerical control machines. For example, the forming gear grinding machine, computer numerical control (CNC) gantry key milling machine, and the cutting line double-side shearing equipment in the leading equipment of China Baosteel's full and heavy plate all adopt the hydrostatic guide rail technology on the main guide rail movement [8]. At present, in the theoretical research on hydrostatic guide rail technology, many Chinese researchers use the finite element method to study and analyze the oil film between the guide rail, as well as the dynamic and static performances of the guide rail. Also, research on solving the calculation model and method of bearing capacity and stiffness of oil film is done, and some fruitful results are achieved.

In order to provide reference and guidance for the optimization design of hydrostatic guide rail, the impact on the performance of hydrostatic guide rail is analyzed by simulating the internal flow field of the guide rail oil chamber. Based on the theory of fluid lubrication and Reynolds equation, a 3D mathematical model of the oil film is established through the finite element method of fluid dynamics. This model is based on the assumption of conditions and the calculation of specific values. Through the calculation, the distribution of the static pressure of the oil film between the guide rails, as well as the distribution law of the flow velocity of the hydraulic oil flow field, can be clarified. The flow field inside the guide oil chamber is simulated. The simulation results are compared with the theoretical calculation results of the traditional equations. Then, the impacts of different oil film thickness and different input pressure parameters of oil inlet on the performance of guide rail are discussed, and the specific rules between them are analyzed. For example, in oil films, the higher its thickness is, the smaller its bearing capacity. Besides, its bearing capacity will increase with the increase in oil supply pressure. Simulation experiments reveal how parameters affect the performance of guide rail. The results can direct the optimization of guide rail design, which is of considerable significance to improve the stability and rigidity of the guide rails.

2 Method

2.1 Text Layout

The hydrostatic guide rail uses the special oil supply equipment to deliver the lubricating oil with an absolute pressure to the hydrostatic oil cavity between two relative moving guide rails, thus forming a lubricating oil layer with absolute pressure between the guide rails. Moreover, the pressure difference between the upper and lower hydrostatic oil cavities can balance the external load on the hydrostatic guide rail. The positioning platform system of the X-axis static pressure guide of the five-axis free surface NC machine is taken as the research object, and the static pressure guide system is designed and calculated. According to the fluid lubrication theory and the Reynolds equation, the oil film in the rectangular oil cavity of the guide rail is analyzed through the finite element method. Meanwhile, the oil film of the guide rail is calculated and simulated by the finite element software FLUENT to obtain the oil-film pressure distribution and oil velocity distribution of the hydrostatic guide rails. According to the theory of fluid lubrication and Reynolds equation, first, the mathematical model of the hydrostatic guide

rail is established. The flow of hydrostatic guide rail hydraulic oil can be regarded as the flow of plate gap. The flow diagram of the plate gap is shown in Fig. 1 below, where 1 is a static block, and 2 is a moving block. According to this flow pattern, the Hagen-Poiseuille equation between the oil pads of the hydrostatic guide rail can be calculated. L is the length of two parallel plates, and the unit is m; b is the width, and the unit is m; h is the height of the gap, and the unit is m, that is, the thickness of the oil film. When the thickness of the oil film is far less than the width, the flow along the width direction can be ignored. The flow is due to the pressure difference between P_1 and P_0 because there is no relative motion between the two plates.

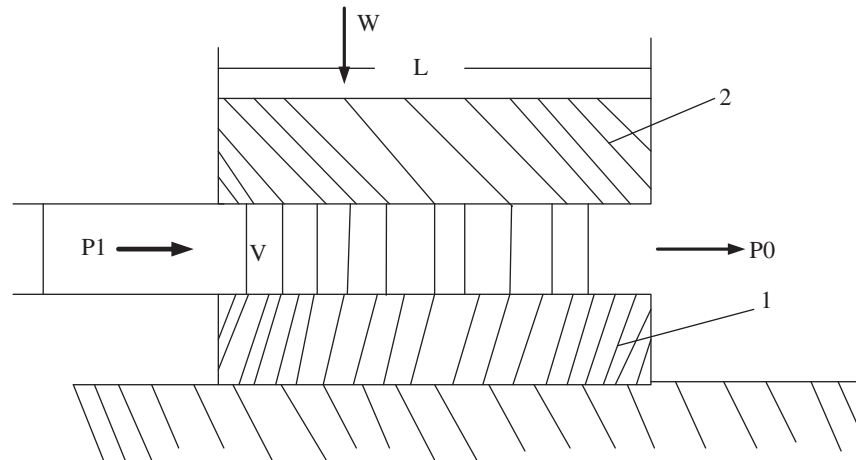


Figure 1: Plate gap flow diagram

A numerical method based on ANSYS Workbench is proposed. First, the Geometry module is used to build the geometry model of the fluid domain, and the Meshing module is used to divide the fluid domain mesh and define the boundary conditions. Through the FLUENT module, the flow field is analyzed. Also, the pressure distribution of the oil film surface in the pressure cavity, the throttle hole, and the micro clearance is obtained. The bearing capacity of the oil film is obtained through integration, and the stiffness of the hydrostatic guide rail is calculated by the method of digit by digit. The impacts of oil supply pressure, orifice diameter, and oil film clearance on the stiffness characteristics and bearing capacity are summarized. The optimum working range of oil film clearance is determined. The pressure distribution of the oil film surface in the fluid domain is coupled to the moving slide in the solid domain. The static characteristics of the moving slide under the flow field pressure and external load are obtained through the fluid-solid coupling analysis. Thus, the strength check of the static pressure guide is completed.

First, the flow in the hydrostatic guide rail is modeled by mathematics and calculated by numerical method. If the flow in the guide rail can be regarded as a 3D steady and incompressible flow, the Reynolds number Re is calculated. Reynolds number is a dimensionless number that can be used to describe the flow of fluid. $Re = \rho v d / \mu$, where v , ρ , and μ are the velocity, density, and viscosity coefficient of the fluid, respectively, and d is a characteristic length. For example, if the fluid flows through a circular pipe, d is the equivalent diameter of the pipe. Reynolds number can be used to distinguish whether the flow of fluid is laminar or turbulent, and also to determine the resistance of the flow of objects in the fluid [9]. The coordinate system indicates that the hydraulic oil and its boundary are static; hence, its speed is zero. For steady flow, the relative velocity is adopted. If the operating environment is under standard atmospheric pressure, the continuity equation and momentum conservation equation can be derived as Eqs. (1)–(3):

$$f_x - \frac{1}{\rho} \frac{\partial p}{\partial x} + v \nabla^2 u = \frac{du}{dt} = \frac{\partial u}{\partial t} + u \frac{\partial u}{\partial x} + v \frac{\partial u}{\partial y} + w \frac{\partial u}{\partial z} \quad (1)$$

$$f_y - \frac{1}{\rho} \frac{\partial p}{\partial y} + v \nabla^2 v = \frac{dv}{dt} = \frac{\partial v}{\partial t} + u \frac{\partial v}{\partial x} + v \frac{\partial v}{\partial y} + w \frac{\partial v}{\partial z} \quad (2)$$

$$f_z - \frac{1}{\rho} \frac{\partial p}{\partial z} + v \nabla^2 w = \frac{dw}{dt} = \frac{\partial w}{\partial t} + u \frac{\partial w}{\partial x} + v \frac{\partial w}{\partial y} + w \frac{\partial w}{\partial z} \quad (3)$$

In (1–3), ν represents the kinematic viscosity of hydraulic oil; u , v , and w respectively represent the velocity components of velocity vector in different directions, i.e., the x , y , and z directions; f is the mass force; p is the pressure, and d is the density. If f_x , f_y , u , and w are zero, the simplified N–S equation can be obtained as Eqs. (4)–(6):

$$-\frac{1}{\rho} \frac{\partial p}{\partial x} = 0 \quad (4)$$

$$-\frac{1}{\rho} \frac{\partial p}{\partial y} + \nu \frac{\partial^2 v}{\partial z^2} = 0 \quad (5)$$

$$-\frac{1}{\rho} \frac{\partial p}{\partial z} = 0 \quad (6)$$

The above equations are analyzed and resolved. According to the boundary conditions of $z = 0$ and $z = h$, the velocity equation in the Y -direction can be deduced as Eq. (7):

$$v = \frac{\Delta p}{2ul} \times z^2 + \frac{\Delta p}{2ul} \times hz \quad (7)$$

Furthermore, the volume flow of the plate gap can be calculated by Eq. (8).

$$Q_s = \int_A v(z) dA = b \int_0^h v(z) dz = \frac{\Delta p h^3 b}{12ul} \quad (8)$$

Through the above Eq. (8), the pressure Eq. (9) of the entire oil film surface can be obtained as follows:

$$W_0 = \int_A (p_1 - p_0) dA \quad (9)$$

Δh means the increment increases to the oil film thickness. According to the above equation, the corresponding bearing capacity can be calculated and expressed with W_2 . The static stiffness equation of hydrostatic guide rail at $h = h_1$ can be deduced as Eq. (10):

$$k_0 = \frac{W_1 - W_2}{h_1 - h_2} \quad (10)$$

The central-difference is adopted to discretize the control equations of the guide rail. First, the oil film flow field must be discretized. Fig. 2a illustrates that the grid is sparsely divided to facilitate the description of the problem. The X -direction is divided into n columns, and the Y -direction is divided into m rows. The internal pressure of the oil cavity forming the matrix of m and n is P_a , and the pressure outside the oil seal is 0, which is the same as the atmospheric pressure. The node data are searched and stored as matrices, as shown in Fig. 2b.

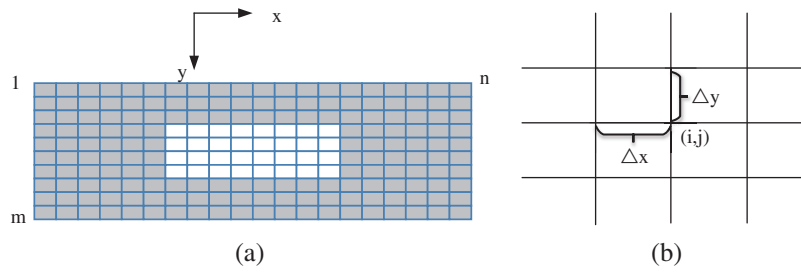


Figure 2: Finite difference discrete grid of a rectangular oil film. a) Discrete grid. b) Node data search

The control equation of the oil seal in the flow field is obtained through the Reynolds equation. It is an elliptical second-order partial differential equation. There are many ways to solve this equation. The finite difference method is easy to program due to its simple format, while the central-difference scheme has two order accuracy; hence, they are widely used. The central finite difference discretizes the oil film control equation, and the finite difference mathematical expression is shown in Eq. (7). The dimensionless processing of (7) can obtain the following equation:

$$\frac{\partial}{\partial \bar{x}} \cdot \left(\bar{h}^3 \frac{\partial \bar{p}}{\partial \bar{x}} \right) + \frac{\partial}{\partial \bar{y}} \left(\bar{h}^3 \frac{\partial \bar{p}}{\partial \bar{y}} \right) = 0 \tag{11}$$

The following equation can be obtained by expanding (11):

$$\frac{\partial \bar{h}^3}{\partial \bar{x}} \cdot \frac{\partial \bar{p}}{\partial \bar{x}} + \bar{h}^3 \cdot \frac{\partial^2 \bar{p}}{\partial \bar{x}^2} + \frac{\partial \bar{h}^3}{\partial \bar{y}} \cdot \frac{\partial \bar{p}}{\partial \bar{y}} + \bar{h}^3 \cdot \frac{\partial^2 \bar{p}}{\partial \bar{y}^2} = 0 \tag{12}$$

According to the central-difference scheme, the first-order and second-order partial derivatives in Eq. (12) are discretized on the grid nodes, and the following equations can be obtained:

$$\left(\frac{\partial \bar{h}^3}{\partial \bar{x}} \right)_{i,j} = \frac{\bar{h}^3_{i,j+1} - \bar{h}^3_{i,j-1}}{2 \cdot \Delta \bar{x}} \tag{13}$$

$$\left(\frac{\partial \bar{h}^3}{\partial \bar{y}} \right)_{i,j} = \frac{\bar{h}^3_{i,j+1} - \bar{h}^3_{i,j-1}}{2 \cdot \Delta \bar{y}} \tag{14}$$

$$\left(\frac{\partial \bar{p}}{\partial \bar{x}} \right)_{i,j} = \frac{\bar{p}_{i,j+1} - \bar{p}_{i,j-1}}{2 \cdot \Delta \bar{x}} \tag{15}$$

$$\left(\frac{\partial \bar{p}}{\partial \bar{y}} \right)_{i,j} = \frac{\bar{p}_{i+1,j} - \bar{p}_{i-1,j}}{2 \cdot \Delta \bar{y}} \tag{16}$$

$$\left(\frac{\partial^2 \bar{p}}{\partial \bar{y}^2} \right)_{i,j} = \frac{\bar{p}_{i+1,j} - 2\bar{p}_{i,j} + \bar{p}_{i-1,j}}{(\Delta \bar{y})^2} \tag{17}$$

The obtained discrete Eqs. (13)–(17) are brought into (12), and the following equations can be obtained:

$$a_{i,j} \cdot \frac{\bar{p}_{i,j+1} - \bar{p}_{i,j-1}}{2 \cdot \Delta x} + \bar{h}_{i,j} \cdot \frac{\bar{p}_{i,j+1} - 2\bar{p}_{i,j} + \bar{p}_{i,j-1}}{(\Delta \bar{x})^2} + b_{i,j} \cdot \frac{\bar{p}_{i+1,j} - \bar{p}_{i-1,j}}{2 \cdot \Delta y} + \bar{h}_{i,j} \cdot \frac{\bar{p}_{i,j+1} - 2\bar{p}_{i,j} + \bar{p}_{i-1,j}}{(\Delta \bar{y})^2} = 0 \quad (18)$$

$$a_{i,j} = \left(\frac{\partial \bar{h}^3}{\partial \bar{x}} \right)_{i,j} \quad (19)$$

$$b_{i,j} = \left(\frac{\partial \bar{h}^3}{\partial \bar{y}} \right)_{i,j} \quad (20)$$

Further arranging the above equations:

$$A_{i,j} \cdot \bar{p}_{i-1,j} + B_{i,j} \cdot \bar{p}_{i+1,j} + C_{i,j} \cdot \bar{p}_{i,j} + D_{i,j} \cdot \bar{p}_{i,j-1} + E_{i,j} \cdot \bar{p}_{i,j+1} = 0 \quad (21)$$

The parameters are respectively represented as:

$$A_{i,j} = \frac{\bar{h}^3_{i,j}}{(\Delta \bar{y})^2} - \frac{b_{i,j}}{2 \cdot \Delta y} \quad (22)$$

$$B_{i,j} = \frac{\bar{h}^3_{i,j}}{(\Delta \bar{y})^2} + \frac{b_{i,j}}{2 \cdot \Delta y} \quad (23)$$

$$C_{i,j} = \frac{-2 \cdot \bar{h}^3_{i,j}}{(\Delta \bar{x})^2} + \frac{-2 \cdot \bar{h}^3_{i,j}}{(\Delta \bar{y})^2} \quad (24)$$

$$D_{i,j} = \frac{\bar{h}^3_{i,j}}{(\Delta \bar{x})^2} - \frac{a_{i,j}}{2 \cdot \Delta \bar{x}} \quad (25)$$

$$E_{i,j} = \frac{\bar{h}^3_{i,j}}{(\Delta \bar{x})^2} + \frac{a_{i,j}}{2 \cdot \Delta \bar{x}} \quad (26)$$

The algebraic equations of Eq. (21) are solved. After the pressure of the flow field is initialized, and the boundary conditions and geometric parameters are brought into the equations; thus, the entire pressure field can be calculated, thereby the bearing capacity of a single oil film.

2.2 Numerical Calculation of Oil Film

2.2.1 Condition Assumption

FLUENT software is used to calculate and analyze the convection field. Before the mathematical modeling and numerical calculation of the internal fluid in hydrostatic guide rail, several assumptions need to be determined. First, the pressure in different parts of the guide rail oil chamber is the same. Second, there is no relative sliding correlation between lubricating oil and solid. Third, the inertial force cannot be calculated. Fourth, the boundary pressure value of the guide oil film is zero. Fifth, while calculating the lubricating oil inside the guide rail, the Reynolds number is not more than 2,300. Afterward, the laminar flow model is used to calculate the internal flow field in the oil chamber. Sixth, the thermal deformation of the worktable and the base will not be considered.

2.2.2 Generate Grid

The upper and lower oil chambers are relative so that only one of them is analyzed. The structure of the oil cavity is simple; thus, the application of a structured network can be constructed into a high-quality grid. The Integrated Computer Engineering and Manufacturing code for Computational Fluid Dynamics (ICEM CFD) is a professional CAE pre-processing software, which has strong CAD model repairability, grid editing technology, automatic midplane extraction, and rich geometry interface [10]. The core idea of the grid generation is topology. The quality of the block strategy determines the quality and speed of the grid generation. Here, the ICEM CFD software is used to complete grid optimization. In ProE, a robust 3D model of hydrostatic pressure is generated. Then, it is transformed into an intermediate format file, which is imported into ICEM CFD for mesh division. Through multiple attempts, the appropriate blocking strategy is chosen, a regular grid is used for transition, and the O-grid is used to divide the throttle holes, thereby obtaining a high-quality structured grid.

2.2.3 Numerical Calculation

FLUENT is a special hydrodynamics software used to simulate and analyze the heat exchange and flow of fluid in complex areas. Its principal function is to calculate, analyze, and predict the flow field and temperature field [11]. Through CFD simulation, the state of the fluid flow process can be analyzed and displayed; the flow performance of the fluid in the simulation area can be accurately predicted; by adjusting various parameters, the optimal parameters of the corresponding process can be obtained [12]. In essence, as a solver, the functions provided by FLUENT mainly include: pre-processing (importing mesh model, providing physical model, and applying boundary conditions and material characteristics), solution, and post-processing [13]. Before using FLUENT, first, the detailed solution scheme is analyzed according to the required physical problems. After importing the grid file into FLUENT, the grid quality and the unit will be rechecked, and the solution parameters will be set after confirming that there is no error. The parameters include material properties, model, solver, boundary conditions, under-relaxation factor, residual setting, and initial flow field. For flow field analysis, only the physical properties of fluid materials need to be set. Whether the liquid flow is laminar or turbulent is a principal concern of model selection. The flow pattern is judged through the Reynolds number: if the number is less than 2,000, the flow will be laminar; if the number is more than 4,000, the flow will be turbulent. The calculation of Reynolds number R_e is shown in Eq. (27). The parameters are calculated to obtain the Reynolds number of each part of the flow field of the supporting element.

$$R_e = \frac{4\rho Q}{\mu Y} \quad (27)$$

where ρ is the oil density, Q is the oil flow, μ is the dynamic viscosity, and Y is the wet cycle.

According to the calculation results, only the gravity in the Z-direction is considered. Then, the Laminar turbulence solution model is chosen; the hydraulic oil dynamic viscosity is set to 0.027 Pas and expressed with μ . Its density ρ is set to 900 kg/m³. Then, the boundary conditions are set, and the oil inlet is pressure-inlet. The pressure is 167803 Pa, which is evenly distributed in the inlet section. The inlet height and diameter are 100 mm and 6 mm, respectively. H is height, and D is the diameter. The position of the oil outlet is pressure-outlet, the pressure is 0 Pa, and the velocity on the solid wall meets the condition of no sliding. Then, the rectangular coordinate system, which coincides with the axis, is established and expressed by (x, y, z) . The rectangular coordinate system is further fixed at the position of the centerline. Then, it is initialized to solve the problem.

FLUENT provides two types of solvers: pressure-based solvers and density-based solvers. The 3D implicit steady-state solvers based on pressure are selected [14]. For the solution algorithm, the simple algorithm is selected considering the application range, convergence speed, and calculation accuracy [15].

The under-relaxation factors of pressure, density, body forces, momentum, and energy are set to 0.3, 1, 1, 0.7, and 0.8, respectively. Meantime, the continuity residuals are set as 10^{-5} , speed residuals as 10^{-4} , and energy residuals as 10^{-6} , and the residuals monitoring chart is opened. In order to accelerate the convergence, the velocity and temperature of the flow field are initialized to 0 and 293.15 K, respectively. After initialization, the number of iteration steps is set to 3,000. When all residuals are nearly stable after iteration to 2,000 steps, the (inlet flow-outlet flow)/inlet flow is found to be -8.25×10^{-7} through monitoring. Therefore, the iteration is completed, and the equation has converged.

According to the final results, the 3D distribution of oil film pressure in hydrostatic guide rail is in the form of a continuous inverted pyramid. From the inner ring of the oil return groove and sealing surface to the outer ring, the pressure of the oil film gradually decreases from the maximum value to zero. The pressure distribution diagram at the section with $x = 0$ and $y = 0$ of the rectangular oil chamber is shown in Figs. 3 and 4, respectively. When $x = 0$, the pressure in each region of the cavity is the same. The pressure from the oil seal to the oil cavity edge is nonlinear, and the pressure increases gradually from low to high. When $y = 0$, the pressure in each area of the oil chamber is the same. The pressure from the oil seal to the oil cavity edge is also nonlinear, and the pressure increases gradually from low to high. Also, the flow rate of liquid from the orifice to the oil chamber is more significant than that from other places. From the oil film to the outside, the flow rate decreases gradually, and there will be vortex near the oil inlet of the throttle. At the junction of the oil pad and the four corners of the oil chamber, the flow rate is the fastest.

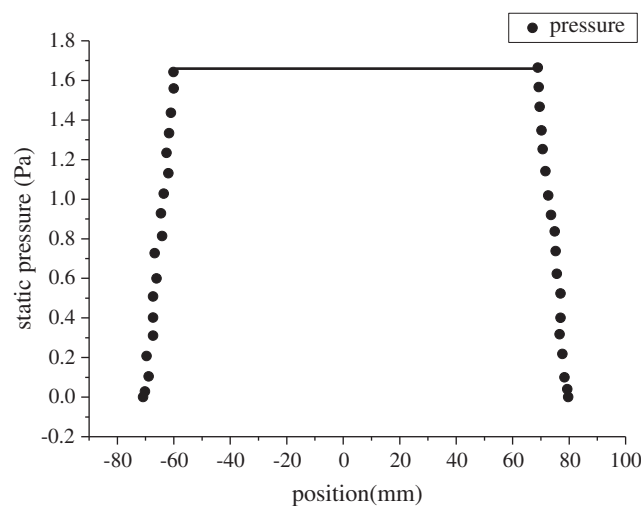


Figure 3: Pressure surface distribution of section $x = 0$

3 Simulation Results

3.1 Impact of Grid Density on Oil Film Pressure, Temperature, and Thickness

The impacts of grid density on oil film pressure, temperature, and thickness are shown in Figs. 5–7, respectively. The grid density has no essential impact on the changing trend of oil film pressure, temperature, and thickness, but makes its value change to some extent. With the increase in grid density, the pressure of the oil film increases, the temperature of the oil film decreases slightly, the thickness of the oil film increases, and the maximum temperature is about 60°C .

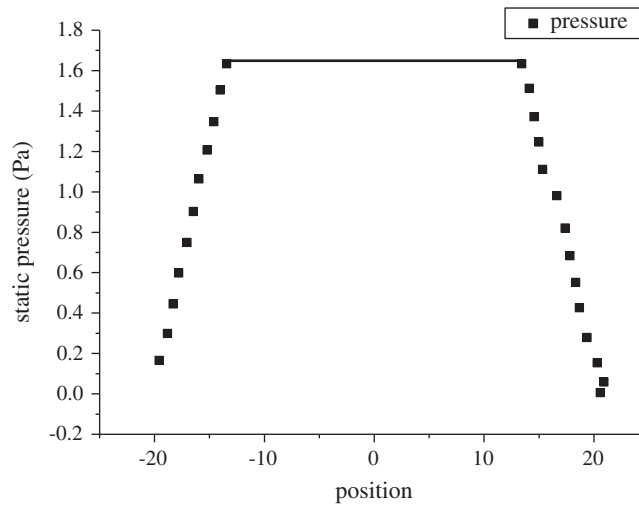


Figure 4: Pressure surface distribution of section $y = 0$

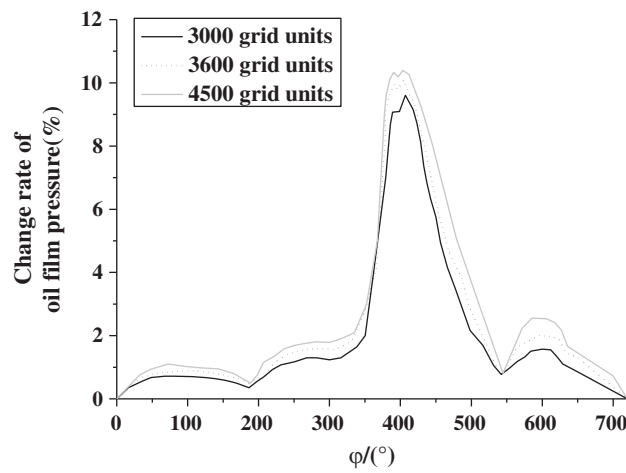


Figure 5: Effect of grid density on oil film pressure

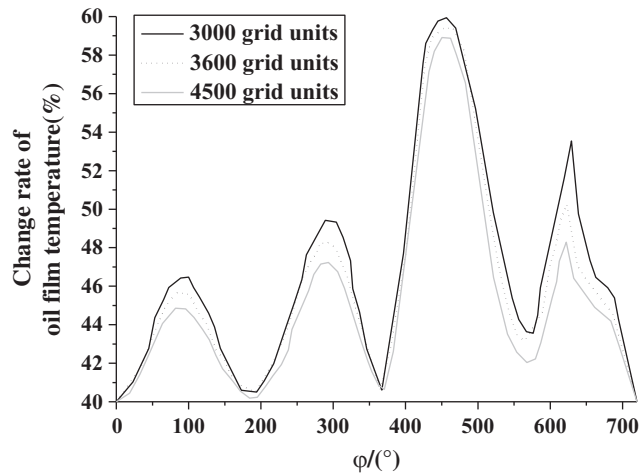


Figure 6: Impact of grid density on oil film temperature

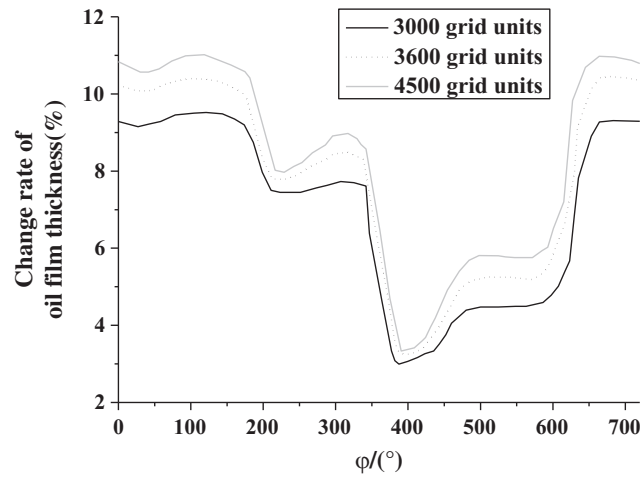


Figure 7: Impact of grid density on oil film thickness

3.2 In-Line Style

The load of the hydrostatic guide rail platform is 350 kg, and its weight is 95 kg, which is carried out by applying two static pressure guide rails. Besides, there are three oil cavities on the top and the bottom of each guide rail, and the primary function of the oil chamber on its side is to guide. The total weight of the six oil chambers is the same, 445 kg. Moreover, the positive load value of each hydrostatic oil chamber is 74.166 kg, which is expressed by F_b [16,17]. Therefore, the load of each oil chamber is 741.66 N. The equation for calculating the bearing capacity of oil film is as Eq. (28):

$$W = A_e P_s = A_e (ap) = A_e \frac{P}{1 + kh^3} \quad (28)$$

In Eq. 11, the impactful bearing area of the guide rail is represented by A_e , and the product of liquid resistance and leakage coefficient is represented by K .

The equation for the flow rate of a single oil chamber is Eq. (29). In Eq. (29), the dynamic viscosity of hydraulic oil is represented by μ , h represents the thickness of oil film, and p_r represents the pressure of the oil chamber.

$$Q_s = \frac{h^3 p_r}{6\mu} \left(\frac{B+b}{L-1} + \frac{L+1}{B-b} \right) \quad (29)$$

The equation for calculating the oil film stiffness is Eq. (30):

$$K = 3 \left(1 - \frac{p_r}{P_s} \right) \times \frac{W}{h} \quad (30)$$

The FLUENT software is used to calculate the bearing capacity of the upper surface of the oil film in the Z-direction. Through the proposed method, the supporting force on the top surface of the oil film of the guide rail is calculated, and its value is 730.64 N as shown in Tab. 1. However, the theoretical result obtained through the above equations is 740.64 N. A comparison between the two results finds that the error is only 1.3%. The calculation results of the proposed method are similar to those of the finite element method, which is in line with the actual situation.

Table 1: Oil film support force on the oil film surface

Simulation data	Theoretical data	R squared change	Error value
730.64 N	740.64 N	10	1.3%

3.3 Comparison and Verification of Design Scheme before and after Optimization

According to the previous optimization results, through the ANSYS Workbench finite element software, the numerical simulation is verified. The comparison and verification of the design scheme before and after optimization are shown in Tab. 2. The overall scores of the design scheme before and after the optimization are 57.2356 and 67.3425, respectively, which increases by 10.1069.

Table 2: Comparison of schemes before and after optimization

Numerical value	Design scheme before optimization	Design scheme after optimization
Overall weight (Kg)	416.75	390.53
Maximum deformation (um)	0.4926	0.4773
Maximum stress (Mpa)	1.2046	0.9975
Comprehensive score	57.2356	67.3425

3.4 Correlation between Oil Film Thickness and Oil Film Bearing Capacity

By integrating the pressure on the surface of the oil film of the hydrostatic guide rail, the bearing capacity simulation data of the hydrostatic guide rail can be obtained, and the theoretical data results of the bearing capacity can be calculated. When the hydrostatic guide rail is under constant oil supply pressure, the oil supply pressure here is determined as 167803 Pa. The correlation between the oil film thickness and the bearing capacity is shown in Fig. 8. Fig. 8 illustrates that the theoretical data results are similar to the experimental simulation results. There is a reverse correlation between the oil film thickness and the bearing capacity, that is, the higher the oil film thickness is, the smaller the bearing capacity of the oil film is. The trend is nonlinear.

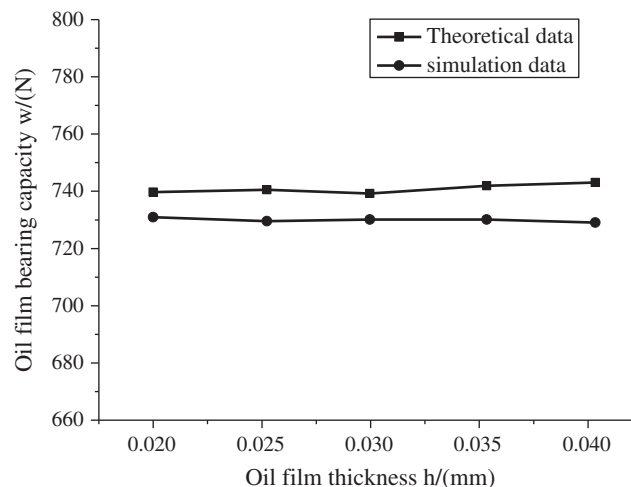


Figure 8: Bearing capacity at different film thicknesses

3.5 The Correlation between the Thickness of Oil Film and the Mass Flow at the Inlet of the Oil Chamber

Because the flow rate of hydrostatic guide rail can show the consumption of hydraulic oil when the hydrostatic guide rail is working, it is calculated here. There are two calculation methods. The first method is to integrate the flow rate in the boundary area of fluid inlet or outlet. The second way is through the traditional theoretical calculation equation. The oil supply pressure here is determined as

167803 Pa. The correlation between the film thickness and the flow rate of the hydrostatic guide is shown in Fig. 9 below. Fig. 9 shows that the theoretical data results are similar to the experimental simulation results. There is a positive correlation between the oil film thickness and the mass flow of the liquid, that is, the mass flow of the liquid will increase with the increase in the oil film thickness. The trend is massive and nonlinear.

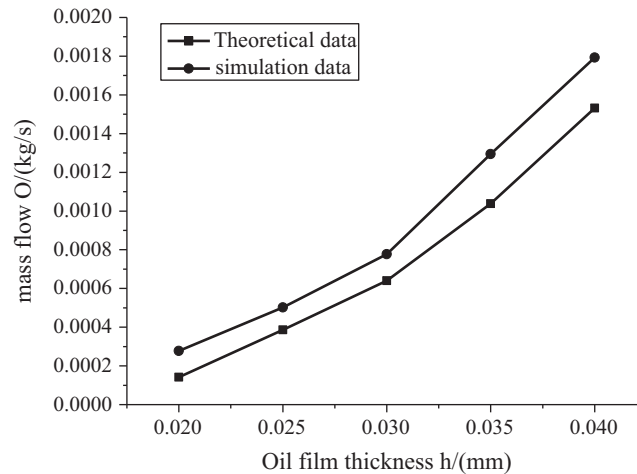


Figure 9: Mass flow rate of oil inlet with different oil film thickness

3.6 The Correlation between the Oil Supply Pressure of the oil Chamber and the Bearing Capacity of the Oil Film

When the structure of hydrostatic guide rail is stable, and the structure design parameters are set, the oil film thickness of hydrostatic guide rail can be kept stable at 0.025 mm all the time by adjusting the restrictor. Afterward, the oil supply pressure of the hydrostatic guide rail is changed, and its change range is set between 1 MPa and 2.5 MPa. 0.5 MPa is set as a variable unit. Then, the performance parameters of a single rectangular hydrostatic guide under different pressure values are calculated before the change rule of its performance parameters is analyzed. The oil film thickness here is determined to be 0.025 mm. The correlation between oil supply pressure and membrane bearing capacity is shown in Fig. 10 below. The theoretical data results and simulation experimental results are similar, and the results obtained by these two different methods reflect the same correlation. Therefore, the bearing capacity of the oil film has a positive correlation with the oil supply pressure; that is, the bearing capacity of the oil film will increase with the increase in the oil supply pressure.

3.7 The Correlation between Film Thickness and Film Stiffness

When the hydrostatic guide rail is supplied with constant pressure oil, the pressure on the surface of the oil film of the hydrostatic guide rail is integrated. Through this method, the simulation data of bearing capacity are obtained, and the theoretical data are obtained through the traditional equation. Then, the stiffness of the rectangular oil film guide rail under different oil film thickness is calculated through the traditional equation. The oil supply pressure here is determined as 167803 Pa. The correlation between oil film thickness and oil film stiffness is shown in Fig. 11 below. Fig. 11 illustrates that the difference between the theoretical data results and the experimental simulation results is minimal, and the results are very close. The results of these two different methods show the same correlation. The correlation between oil film thickness and oil film stiffness is reversed; that is, the oil film stiffness will gradually decrease with the increase in oil film thickness. The trend is massive and nonlinear.

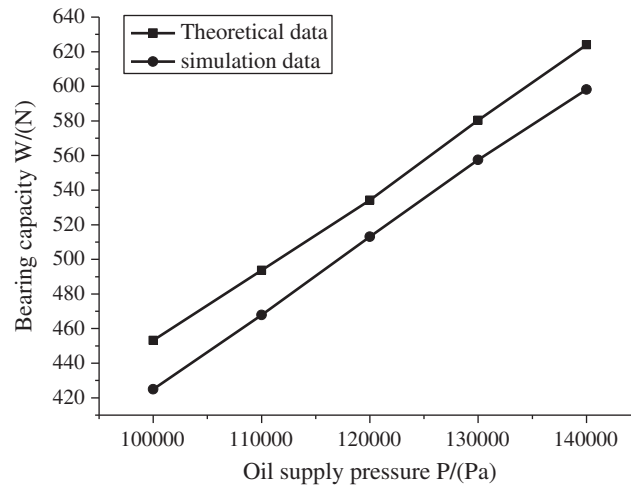


Figure 10: Correlation between oil supply pressure and oil film bearing capacity

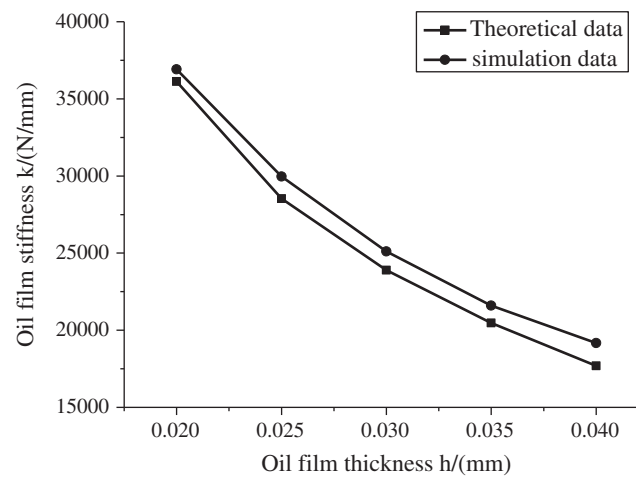


Figure 11: Oil film stiffness curve with different oil film thickness

3.8 Correlation Between Oil Supply Pressure and Oil Film Stiffness

If the oil supply pressure is different, the rectangular oil chamber of the hydrostatic guide rail is different. Therefore, the range of change is set between 1 MPa and 2.5 MPa. Then, the bearing capacity is calculated when the oil film thickness is 0.02 mm. Afterward, the bearing capacity is calculated when the oil film thickness is 0.025 mm. The traditional calculation equation is applied to calculate the rigidity of the oil film of the rectangular oil cavity guide rail under different oil supply pressures. The correlation between oil supply pressure and oil film stiffness is shown in Fig. 10 below. The figure suggests that the theoretical data results and simulation experiment results are similar, and the results obtained by the two different methods indicate the same correlation. There is a positive correlation between the film thickness and the film stiffness; in other words, the film stiffness will increase with the increase in the oil supply pressure. The trend is massive and nonlinear.

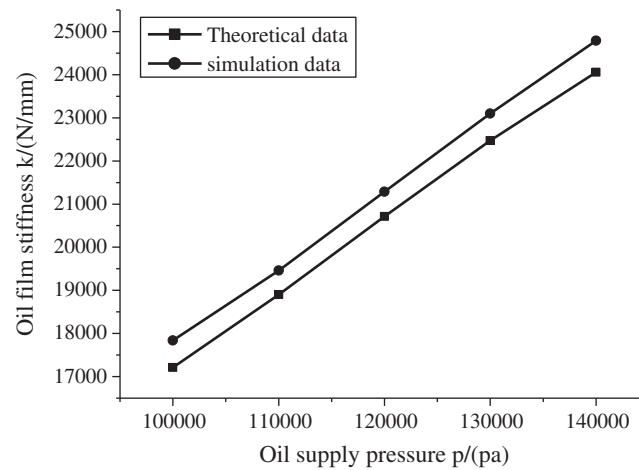


Figure 12: Correlation between oil supply pressure and oil film stiffness of the hydrostatic guide

3.9 Comparison between Theoretical and Experimental Data of Dimensionless Bearing Capacity Coefficient

The above measurement data are transformed and fitted to plot the experimental bearing capacity curve. The comparison of the dimensionless bearing-capacity coefficient and experimental data is shown in Fig. 13. The connection between the two experimental curves can reveal the approximate experimental bearing-capacity coefficient curve. There is an absolute deviation between the experimental curve and the theoretical curve, which is caused by the impact of internal forces. Meanwhile, many error items, such as measurement error of measuring equipment, manufacturing error of guide rail, uncertainty error of oil supply pressure of oil pump, are also coupled in the experimental curve. However, these errors are smaller than the above experimental principle errors and have less impact on the data. The trend of the experimental curve suggests that the measurement results are consistent with the numerical trend of the theoretical curve, which has a particular reference value.

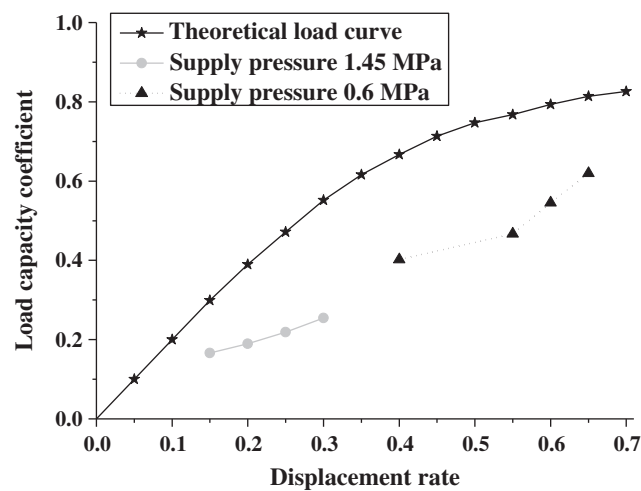


Figure 13: Experimental curve and theoretical curve of the dimensionless bearing capacity coefficient

4 Discussion

With the continuous progress of science and technology, ultra-precision machining technology becomes more common and widespread, playing a vital role in China's industry and national defense. This technology is valued globally; many experts and scholars have researched it deeply, and some fruitful results are achieved. The guide rail components with high precision play a decisive role in the precision of ultra-precision machine tools. A high-precision guide rail component can also improve the accuracy of the linear motion platform and relative position of the machine tool [18–20]. Hydrostatic guide rail has many advantages, such as high precision, high stiffness, and long life; therefore, it has an extensive range of applications. For factories, the fundamental problem of the hydrostatic guide rail technology is the supporting force and the rigidity of the guide rail oil film [21]. In order to improve the stability of oil films, the load-carrying capacity and the rigidity of resisting the external load must be optimized. Besides, the cyclic alternating stress in the bearing area of hydrostatic guide rail will also affect the performance of guide rail. Guellal et al. solved the problem in the framework of the velocity-pressure equation of the finite volume method based on the standard SIMPLER algorithm, who also studied the impact of control parameters (geometry, hydrodynamics, and heat) on fluid flow and heat transfer [22]. Many researchers also investigated the impacts of different parameters (Rayleigh number, buoyancy number, optical thickness, and Lewis number) on fluid flow, heat, and mass transfer [23,24].

Therefore, by simulating the flow field inside the guide oil chamber, the impact of the method on the performance of hydrostatic guide is studied, and the pressure oil film finite element model of the axis hydrostatic guide of ultra-precision machine tool is established. According to the theory of fluid lubrication and the Reynolds equation, the model is assumed to be conditional and calculated with a specific numerical value. The calculations help analyze the oil film pressure and flow field between guide rails. Afterward, the flow field inside the guide oil chamber is simulated. Through the traditional empirical equation, the correctness of the simulation results is verified; thus, the impacts of different structural design parameters and environmental factors on the performance of hydrostatic guide rail are determined. Besides, the impacts of different oil film thickness and different input pressure parameters of the oil inlet on the performance of guide rail are discussed and analyzed. There are specific rules between them.

Through the proposed method, the supporting force on the top surface of the oil film of the guide rail is calculated, and its value is 930.64 N. However, the theoretical result is 740.64 N. A comparison between the two results finds that the error rate is only 1.3%. Hence, the calculation results of the proposed method and the finite element method are not much different, which is in line with the actual situation. The simulation results are similar to the traditional theoretical calculation results, the pressure of the rectangular oil cavity changes little, and the streamline distribution is proper. However, at the throttle, there is a flow of pressure energy. A greater thickness of the oil film indicates a smaller bearing capacity. The oil film thickness and the mass flow of the liquid share a positive correlation. The mass flow of the liquid will increase with the increase in the oil film thickness. The bearing capacity of oil film shares a positive correlation with oil supply pressure; that is, the bearing capacity of oil film will increase with the increase in oil supply pressure. Besides, there is a positive correlation between the film thickness and the film stiffness; in other words, the film stiffness will increase with the increase in the oil supply pressure.

The impacts of oil film thickness and other parameters on the performance of the guide rail are analyzed, and the rules between them are clarified, which can provide a positive reference for the follow-up optimization design of machine tools and guide rails. The results have specific innovations. According to the actual working condition of the hydrostatic guide rail, the hydrostatic guide rail system is designed and calculated. Based on the theory of fluid lubrication and Reynolds equation, the oil film in the rectangular oil cavity of the guide rail is analyzed by the finite element method. In the meantime, with the aid of the finite element software, the oil film pressure distribution and oil velocity distribution of the hydrostatic guide are obtained. In the above experiment, only the finite element method is used to get

the simulation results of the hydrostatic guide rail. Due to the limited conditions, it is impossible to manufacture the actual ultra-precision machine tools for experimental verification, which will be perfected later.

5 Conclusion

The results of the oil film support force calculated by the simulation analysis method and the traditional formula are almost the same. The result of the traditional algorithm is 740.63 N, and the simulation result is 730.64 N, showing that the model simulation method applied has absolute accuracy. The experimental results show that the bearing capacity of oil film is affected by the thickness of oil film and the pressure of oil supply. In addition, the oil supply pressure will also affect the oil film stiffness, and there are a specific correlation and laws between them. The above results can provide theoretical guidance for the optimization of machine tools and guide rails in the future. However, this study only obtains the simulation results of the hydrostatic guide rail by establishing the finite element model, which has not been verified by the ultra-precision machine tool in practical application and lacks certain experimental conditions. In future experiments, the model will be analyzed in the actual application of machine tools to enhance the depth and reliability of the results.

Acknowledgement: Acknowledgements and Reference heading should be left justified, bold, with the first letter capitalized but have no numbers. Text below continues as normal.

Funding Statement: The author(s) received no specific funding for this study.

Conflicts of Interest: The authors declare that they have no conflicts of interest to report regarding the present study.

References

1. Ghassemi, M., Chen, Q., Yang, C. (2017). The influence magnitude and rise time of applied voltage and the type of oil on streamer growth in a wet-mate DC connector. *IEEE Transactions on Dielectrics and Electrical Insulation*, 24(3), 1646–1656. DOI 10.1109/TDEI.2017.006448.
2. Huang, H., Liu, J., Liu, X., Xiao, J., Zhong, S. et al. (2016). Physical simulation of the interlayer effect on SAGD production in mackay river oil sands. *Fuel*, 183, 373–385. DOI 10.1016/j.fuel.2016.05.120.
3. Jun, Z., Dun, L. V., Qian, J., Chen, Y. L. (2015). Motion straightness of hydrostatic guideways considering the ratio of pad center spacing to guide rail profile error wavelength. *International Journal of Advanced Manufacturing Technology*, 82(9), 1–9. DOI 10.1007/s00170-014-6601-1.
4. Jakub, T., Pavel, B., Lucie, V., Slouka, Z. (2016). Electric field driven addressing of oil-in-water droplets in the presence of gradients of ionic and nonionic surfactants. *IEEE Transactions on Industry Applications*, 52(6), C1–4524. DOI 10.1109/TIA.2016.2619619.
5. Nattan, R. C., Cataluña, H. A., Vielmo, H. A. (2015). Analysis of the effect on the mechanical injection engine using doped diesel fuel by ethanol and bio-oil. *International Review of Mechanical Engineering*, 9(2), 124.J.
6. Zhu, Y. M., Yi, J. Y., Xu, M., Chen, Z., Yang, S. H. et al. (2019). Quantum chemical simulation and laboratory testing of the curing mechanism and performance of resin bio-oil. *International Journal of Pavement Engineering*, 17, 1–20.
7. Xiao, C., Huang, K., Liu, H. (2017). Effect of change in aqueous-to-oil phase ratio on the performance of mixer-settler in extraction processes. *Chinese Journal of Process Engineering*, 17(5), 885–892.
8. Deng, M. R., Guo, H. X., Xiong, S. Y. (2017). Influence of building chambers on internal ventilation and corresponding simulation analysis. *Journal of South China University of Technology*, 45(5), 74–81.
9. Kong, X., Chen, L., Li, Y. (2015). Numerical analysis of acoustic and resistance performance of muffler in refrigeration compressor's discharge pipe. *Transactions of the Chinese Society of Agricultural Engineering*, 31(5), 59–64.
10. Dong, W. J., Li, B. Z., Guo, W. C., Zhou, Q. Z. (2019). Deformation analysis of hydrostatic guideways based on the cantilever plate bending calculation method. *Tribology Transactions*, 62(6), 1142–1154. DOI 10.1080/10402004.2019.1669755.

11. Li, S. N., Wei, L. J., Wei, X. P., Yang, J. H. (2020). Change in oil pressure in piston chamber of a radial piston pump pre-compression area when considering the compressibility of oil. *International Journal of Fluid Machinery and Systems*, 13(2), 463–475. DOI 10.5293/IJFMS.2020.13.2.463.
12. Quan, L., Gao, H., Guo, C., Che, S. (2020). Assessment of the dynamics flow field of port plate pair of an axial piston pump. *Processes*, 8(1), 86. DOI 10.3390/pr8010086.
13. Chen, L., Cui, B. Y., Zhao, J. H., Gao, D. R. (2018). Influence of parameters of PM controller on vibration performance of liquid hydrostatic guide-way system. *Noise & Vibration Worldwide*, 49(4), 140–146. DOI 10.1177/0957456518781856.
14. Xiang, S., Deng, M., Li, H. M., Du, Z. C., Yang, J. G. (2019). Cross-rail deformation modeling, measurement and compensation for a gantry slideway grinding machine considering thermal effects. *Measurement Science and Technology*, 30(6), 065007. DOI 10.1088/1361-6501/ab1232.
15. Shah, M. Z. M., Basuno, B., Abdullah, A. (2020). Comparative study on several type of turbulence model available in ANSY-fluent software for ONERA M6 wing aerodynamic analysis. *Journal of Advanced Mechanical Engineering Applications*, 1(1), 9–19.
16. Wang, X., Qin, C., Liu, J. (2019). Study on the simulation optimization of guided waves for the inspection of the pitting in pipeline. *Yi Qi Yi Biao Xue Bao/Chinese Journal of Scientific Instrument*, 40(1), 166–174.
17. Meng, A. H., Song, J., Han, S. S., Pan, N. (2015). Simulation research on improving the efficiency of piston pump of automotive ESP. *Chinese Hydraulics & Pneumatics*, 4, 24–28.
18. Yu, Z. L., Guo, H. T., Shao, Q., Ma, L., Xu, T. et al. (2016). Numerical simulation of impingement cooling double chamber model with cross coolant hole arrangements. *Journal of Computational and Theoretical Nanoscience*, 13(3), 2049–2055. DOI 10.1166/jctn.2016.5154.
19. Wen, T., Dong, S., Gong, Z., Li, L. Q., Zheng, L. et al. (2017). Structure design of sweeping type bionic olfactory detection chamber and its flow field performance simulation and verification. *Nongye Gongcheng Xuebao/transactions of the Chinese Society of Agricultural Engineering*, 33(10), 78–85.
20. de Carvalho, M. F., de Sousa, A. G., Domingues, R. O., de Araújo, R. P., Ferreira, R. A. S. et al. (2016). Internal coating of oil refining pipes with alumina from the recycling process of aluminum anodizing. *Materials Science Forum*, 881, 367–372. DOI 10.4028/www.scientific.net/MSF.881.367.
21. Li, K. L., Wang, H. M., Wang, J. X., Zhao, Y. (2017). Analysis of the Internal flow field of low flow resistance coefficient axial flow type check valve. *Journal of Engineering for Thermal Energy & Power*, 32(12), 78–83.
22. Guellal, M., Hamimid, S., Amroune, A., Zeraibi, N. (2011). Effect of a porous layer on the flow structure and heat transfer in a square. *Fluid Dynamics & Materials Processing*, 8(1), 69–90.
23. Parsa, A., Saghiri, M. Z. (2012). Fluid flow behavior of a binary mixture under the influence of external disturbances using different density models. *Fluid Dynamics & Materials Processing*, 8(1), 27–50.
24. Moufekkik, F., Moussaoui, M. A., Mezrhab, A., Naji, H., Bouzidi, M. (2012). Numerical study of double diffusive convection in presence of radiating gas in a square cavity. *Fluid Dynamics & Materials Processing*, 8(2), 129–153.